Gα13 loss in Kras/Tp53 mouse model of pancreatic tumorigenesis promotes tumors susceptible to rapamycin

Mario A. Shields[1,2,4,*], **Christina Spaulding**[1,3], **Anastasia E. Metropulos**[1], **Mahmoud G. Khalafalla**[1], **Thao N.D. Pharm**[1], **Hidayatullah G. Munshi**[1,2,3,*]

[1]Department of Medicine, Feinberg School of Medicine, Northwestern University, 303 E. Superior Avenue, Lurie 3-220 or Lurie 3-117, Chicago, IL 60611, USA

[2]The Robert H. Lurie Comprehensive Cancer Center, Chicago, IL, USA

[3]Jesse Brown VA Medical Center, Chicago, IL, USA

[4]Lead contact

SUMMARY

Gα13 transduces signals from G-protein-coupled receptors. While Gα13 functions as a tumor suppressor in lymphomas, it is not known whether Gα13 is pro-tumorigenic or tumor suppressive in genetically engineered mouse (GEM) models of epithelial cancers. Here, we show that loss of Gα13 in the Kras/Tp53 (KPC) GEM model promotes well-differentiated tumors and reduces survival. Mechanistically, tumors developing in KPC mice with Gα13 loss exhibit increased E-cadherin expression and mTOR signaling. Importantly, human pancreatic ductal adenocarcinoma (PDAC) tumors with low Gα13 expression also exhibit increased E-cadherin expression and mTOR signaling. Treatment with the mTOR inhibitor rapamycin decreases the growth of syngeneic KPC tumors with Gα13 loss by promoting cell death. This work establishes a tumor-suppressive role of Gα13 in pancreatic tumorigenesis in the KPC GEM model and suggests targeting mTOR in human PDAC tumors with Gα13 loss.

In brief

Shields et al. reveal a tumor-suppressive role of Gα13 in the KPC mouse model of pancreatic tumorigenesis. Mouse KPC tumors, as well as human pancreatic tumors, with reduced Gα13 demonstrate increased E-cadherin expression and mTOR signaling. Loss of Gα13 sensitizes KPC tumors to rapamycin and reduces tumor growth *in vivo*.

*Correspondence: h-munshi@northwestern.edu (H.G.M.), mario.shields@northwestern.edu (M.A.S.).

Graphical Abstract
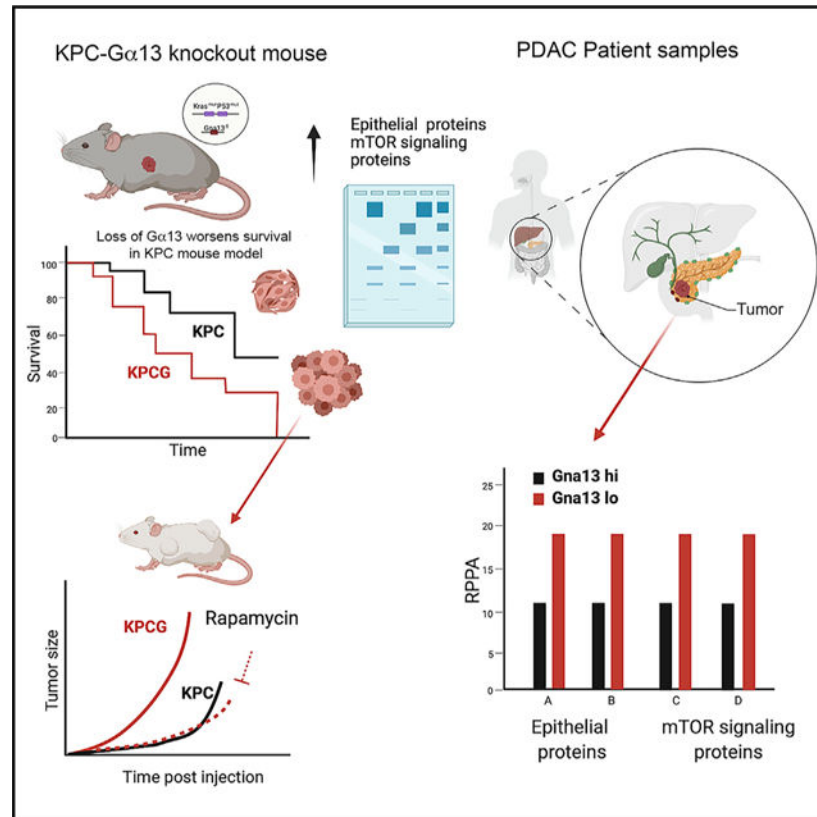
INTRODUCTION

Gα proteins transduce signals from G-protein-coupled receptors (GPCRs) to regulate diverse cellular activities, such as cell growth, differentiation, and survival (Oldham and Hamm, 2008; Syrovatkina et al., 2016). Activating mutations in Gαs, for example, contribute to the development of intraductal papillary mucinous neoplasms (IPMNs) (Molin et al., 2013; Wu et al., 2011), precursor lesions of the pancreas that can progress to pancreatic ductal adenocarcinoma (PDAC) tumors (Farrell and Fernandez-del Castillo, 2013; Matthaei et al., 2011). Pancreas-specific co-expression of mutant *Gnas* and mutant *Kras* cooperate to promote IPMNs in mouse models (Ideno et al., 2018; Patra et al., 2018; Taki et al., 2016), with concurrent loss of Tp53 facilitating progression to PDAC (Patra et al., 2018). While the role of Gαs in pancreatic cancer is now well recognized, the role of other G proteins in pancreatic tumor initiation and progression has yet to be fully defined.

Gα13 plays a critical role in normal and pathological conditions (Kelly et al., 2006, 2007; Kozasa et al., 2011). It is involved in cell-cell and cell-matrix regulation, cytoskeleton organization, and cell migration and invasion (Kelly et al., 2006, 2007; Kozasa et al., 2011). We have shown that targeting Gα13 in pancreatic cancer cells *in vitro* enhances E-cadherin-mediated cell adhesions to decrease cellular invasion in three-dimensional (3D) collagen (Chow et al., 2016). Others have shown that overexpression of Gα13 can induce

cell transformation *in vitro* (Maziarz et al., 2020; Voyno-Yasenetskaya et al., 1994; Xu et al., 1994), suggesting that Gα13 may be pro-tumorigenic *in vivo*. However, studies in mouse models of B cell lymphoma have found that Gα13 functions as a tumor suppressor *in vivo* (Healy et al., 2016; Muppidi et al., 2014; O'Hayre et al., 2016). Loss of Gα13 function in germinal center B cells increases Akt signaling and protects against cell death (Muppidi et al., 2014). Gα13 loss also cooperates with MYC overexpression in germinal center B cells to promote lymphomas (Healy et al., 2016). While these results demonstrate that Gα13 functions as a tumor suppressor in lymphomas (Healy et al., 2016; Muppidi et al., 2014; O'Hayre et al., 2016), it is not known whether Gα13 is pro-tumorigenic or tumor-suppressive in genetically engineered mouse (GEM) models of epithelial cancers. Here, we evaluate the effects of Gα13 loss in the Kras/Tp53 (KPC) and the Kras (KC) GEM models of pancreatic tumorigenesis.

RESULTS

Loss of Gα13 in the KPC GEM model promotes pancreatic tumor development and progression

To investigate the contribution of Gα13 to pancreatic cancer development and progression, we evaluated the effects of Gα13 loss in the LSL-Kras$^{G12D/+}$ × LSL-Trp53$^{R172H/+}$ × Pdx1-Cre (KPC) GEM mouse model. The KPC model is a well-established model that utilizes a pancreas-specific Pdx1 promoter-driven Cre recombinase to knock in the mutant Kras^{G12D} and the mutant p53$^{R172H/+}$ into the endogenous locus in the mouse pancreas (Hingorani et al., 2005). We generated KPC mice with heterozygous and homozygous loss of Gα13 in the mouse pancreas (KPCG$^{fl/+}$ and KPCG$^{fl/fl}$; Figure 1A). The KPCG$^{fl/+}$ and the KPCG$^{fl/fl}$ mice showed decreased pancreatic expression of Gα13 (Figure 1B). At 3 months of age, the KPCG$^{fl/fl}$ and KPCG$^{fl/+}$ mice developed increased lesion burden and increased proliferation (Ki67 staining) compared with the KPC (KPCG$^{+/+}$) mice (Figure 1C). At the survival endpoints, the KPCG$^{fl/fl}$ and KPCG$^{fl/+}$ mice developed well-differentiated tumors with decreased trichrome staining (Figure 1D). There was increased Ki67, CK19, and E-cadherin staining in tumors developing in the KPCG$^{fl/fl}$ and KPCG$^{fl/+}$ mice compared with the KPCG$^{+/+}$ mice (Figure 1D). Co-staining of the tumors for CK19 and Ki67 demonstrated increased proliferation of CK19^{+} cells in the KPCG$^{fl/fl}$ and KPCG$^{fl/+}$ mice (Figure 1D). Notably, there was a significantly reduced survival of the KPCG$^{fl/fl}$ and KPCG$^{fl/+}$ mice compared with the KPCG$^{+/+}$ control mice (Figure 1E). These results suggest a tumor-suppressive role for Gα13 in the Kras/Tp53 mouse model of pancreatic tumorigenesis.

Gα13 is dispensable for tumor development in the KC GEM model

We also evaluated the effects of Gα13 loss in the LSL-Kras$^{G12D/+}$ × Pdx1-Cre (KC) GEM model (Hingorani et al., 2003; Pham et al., 2021). We generated KC mice with heterozygous and homozygous loss of Gα13 in the mouse pancreas (KCG$^{fl/+}$ and KCG$^{fl/fl}$; Figure S1A). The KCG$^{fl/+}$ and the KCG$^{fl/fl}$ mice showed decreased pancreatic expression of Gα13 (Figure S1B). In contrast to the effects of Gα13 loss in the KPC mouse model, the Gα13 loss in the KC mouse did not affect tumor development. There was no difference in the lesion burden in the KC (KCG$^{+/+}$), KCGfl/+, and KCG$^{fl/fl}$ mice at either × or 6 months of age (Figure S1C). While the KCG$^{fl/fl}$ mice demonstrated fewer acinar-to-ductal

metaplasia (ADM) and pancreatic intraepithelial neoplasia (PanIN) 1A lesions, there was no difference in the number of the PanIN1B or PanIN2 lesions between the KCG^{fl/fl} mice and the KCG^{+/+} or the KCG^{fl/+} mice (Figure S1C). There was no difference in Ki67 staining in the pancreas of these mice (Figure S1D). There was also no difference in the survival of KCG^{+/+}, KCG^{fl/+}, and KCG^{fl/fl} mice (Figure S1E). These results indicate that Gα13 loss has differential effects on the growth of Kras-expressing tumors, depending on whether there is co-expression of mutant p53. While Gα13 is dispensable for tumor development in the KC model (Figure S1), loss of Gα13 in the KPC model promotes tumor growth (Figure 1).

Human PDAC tumors with reduced Gα13 expression and tumors developing in the KPCGfi/+ and KPCGfi/fi mice demonstrate increased mTOR signalling

To understand why the KPC mice with Gα13 loss show increased tumor growth and proliferation, we analyzed human reverse-phase protein array (RPPA) data using The Cancer Genome Atlas (TCGA) on the cBioPortal website (Cerami et al., 2012; Gao et al., 2013) (Table S1). We queried for signaling pathways in human PDAC tumors associated with decreased Gα13 expression. We initially evaluated the relationship between E-cadherin and Gα13 in human PDAC tumors. Consistent with the KPC mouse model (Figure 1), human PDAC tumors with low Gα13 expression showed increased E-cadherin protein expression (Figure 2A). Human tumors with reduced Gα13 expression also showed increased expression of β-catenin (CTNNB1) and claudin-7 (CLDN7) proteins (Figure 2A). Increased CTNNB1 and increased CLDN7 are associated with increased differentiation in human PDAC tumors (Lowy et al., 2003; Soini et al., 2012). In addition, there was evidence of increased activation of mammalian target of rapamycin (mTOR) signaling, with increased protein expression of phosphorylated-phosphoinositide dependent protein kinase 1 (p-PDK1 (S241)), mTOR, ribosomal protein S6 (RPS6), and eukaryotic translation elongation factor 2 (EEF2) in human PDAC tumors with reduced Gα13 expression (Figure 2A).

We next evaluated whether our KPC mice with Gα13 loss also exhibited increased mTOR signaling at 3 months and survival endpoints by immunohistochemical staining for mTOR, phosphorylated (p)-mTOR, Rps6, and p-Rps6. Immunohistochemical staining of the lesions at 3 months of age showed that the KPCG^{fl/fl} and KPCG^{fl/+} mice exhibited increased p-mTOR staining, with a trend toward increased p-Rps6 staining, compared with the KPCG^{+/+} mice (Figure 2B). At survival endpoints, KPCG^{fl/fl} tumors demonstrated increased Rps6 and p-Rps6 immunohistochemical staining compared with the KPCG^{+/+} tumors (Figure 2C). Similarly, the KPCG^{fl/+} tumors showed increased mTOR, p-mTOR, and Rps6 immunohistochemical staining at survival endpoints (Figure 2C). We also evaluated the tumor lysates from KPCG^{+/+}, KPCG^{fl/fl}, and KPCG^{fl/+} mice at survival endpoints by western blotting for p-mTOR, mTOR, p-Rps6, and Rps6. Compared with the tumor lysates from the KPCG^{+/+} mice, the tumor lysates from the KPCG^{fl/+} and KPCG^{fl/fl} mice exhibited overall increased mTOR and Rps6 phosphorylation (Figure 2D).

Gα13 loss does not increase mTOR signaling in the KC GEM model

We also evaluated the effects of Gα13 loss on mTOR signaling in the KC model. At survival endpoints, there was no difference in p-mTOR or p-Rps6 staining in the lesions developing in the KCG^{fl/+} and KCG^{fl/fl} mice compared with the lesions in the KCG^{+/+} mice (Figure

S2). These results demonstrate that Gα13 loss in the KPC mouse model, but not in the KC mouse model, increases mTOR signaling.

Cell lines established from KPCGfi/fi mice demonstrate increased tumor growth with increased E-cadherin expression

To evaluate whether targeting mTOR signaling mediates the effects of increased tumor growth following Gα13 loss, we established cell lines from tumors developing in the KPCG$^{+/+}$ and KPCG$^{fl/fl}$ mice. Compared with the KPCG$^{+/+}$ cell lines 2138 and 3213, the KPCG$^{fl/fl}$ cell lines 3458 and 3566 exhibited loss of Gα13 expression (Figure 3A). When embedded in 3D collagen matrix, the KPCG$^{+/+}$ cell lines grew as single cells and showed a spindle-shaped morphology. In contrast, the KPCG$^{fl/fl}$ cell lines grew as compact spheroids in 3D collagen (Figure 3A). When transplanted in syngeneic mice, the KPCG$^{fl/fl}$ cells grew significantly faster and formed larger tumors (Figure 3B). As with the tumors developing in the KPCG$^{fl/fl}$ GEM model, the tumors developing from KCG$^{fl/fl}$ cell lines exhibited increased Ki67 staining (Figure 3C). There was decreased trichrome staining (Figure 3D), increased cytokeratin 19 (CK19) expression (Figure 3D), and increased E-cadherin expression (Figure 3E).

Cell lines established from KCG$^{fi/fi}$ mice fail to form tumors *in vivo*

We also established cell lines from the KCG$^{+/+}$ (2685 and 2005) and KCG$^{fl/fl}$ (1999 and 1930) mice. The KCG$^{fl/fl}$ cell lines showed a near-complete loss of Gα13 expression (Figure S3A). When grown in 3D collagen, the KCG$^{+/+}$ cell lines exhibited spindle-shaped morphology (Figure S3B). In contrast, the KCG$^{fl/fl}$ cell lines failed to grow in 3D collagen (Figure S3B). To evaluate the effect on growth in 3D collagen, the KCG$^{+/+}$ and the KCG$^{fl/fl}$ cell lines were grown in 3D collagen for 7 days, extracted out of collagen, and counted. Compared with the control KCG$^{+/+}$ cell lines, the KCG$^{fl/fl}$ cell lines exhibited significantly reduced growth in 3D collagen (Figure S3B). Similarly, when these cell lines were grown *in vivo*, the KCG$^{fl/fl}$ cells failed to form tumors *in vivo* (Figure S3C). These results indicate that Gα13 loss has differential effects on the growth of Kras-expressing cells, depending on whether there is co-expression of mutant p53. While the loss of Gα13 inhibited tumor growth of KC cell lines *in vivo* (Figure S3), loss of Gα13 in the KPC cell lines promoted tumor growth *in vivo* (Figure 3).

Gα13 loss sensitizes KPC tumors to the mTOR inhibitor rapamycin and reduces tumor growth *in vivo*

In addition to the increased E-cadherin expression, the KPCG$^{fl/fl}$ tumors also showed increased mTOR signaling. There was increased expression of p-Pdk1, Pdk1, p-mTOR, mTOR, p-Rps6, and Rps6 in the KPCG$^{fl/fl}$ tumors compared with the KPCG$^{+/+}$ tumors (Figure 4A). Given the robust activation of the mTOR signaling in tumors established from the KPCG$^{fl/fl}$ cell lines, we evaluated the effects of rapamycin *in vivo*. We treated established KPCG$^{+/+}$ and KPCG$^{fl/fl}$ tumors with vehicle control or rapamycin. Rapamycin significantly decreased tumor growth of both KPCG$^{+/+}$ and KPCG$^{fl/fl}$ tumors, but the effect was particularly pronounced in the KPCG$^{fl/fl}$ tumors (Figures 4B and 4C). Tumors treated with rapamycin showed suppression of the mTOR signaling (Figure 4D). While rapamycin reduced proliferation in the KPCG$^{+/+}$ tumors (Figure 4E), it did not induce apoptosis (Figure

4F). In contrast, while rapamycin did not suppress proliferation of the KPCG^fl/fl tumors (Figure 4E), there was a significant increase in cell death in the KPCG^fl/fl tumors following rapamycin treatment (Figure 4F). Overall, our data demonstrate that the KPC tumors with Gα13 loss are susceptible to treatment with rapamycin.

DISCUSSION

GPCRs are targets of several currently approved therapies (Hauser et al., 2017). There is increasing interest in understanding the role of effectors downstream of GPCRs and determining whether these effectors could be potential therapeutic targets (Hauser et al., 2017). Because GPCRs can signal through Gα13 (Kurose, 2003), many studies have evaluated the contribution of Gα13 to physiologic and pathologic processes (Sriram et al., 2020; Syrovatkina and Huang, 2019; Tutunea-Fatan et al., 2020). These studies, primarily performed in epithelial cancer cell lines, showed that Gα13 functions as a tumor promoter (Chow et al., 2016; Kelly et al., 2006, 2007; Kozasa et al., 2011; Rasheed et al., 2018; Zhang et al., 2018). However, we now show that targeting Gα13 in the Kras/Tp53-driven KPC GEM model results in increased tumor development and decreased survival, indicating that Gα13 has a tumor-suppressive role in pancreatic tumors. Our data agree with the previously published studies showing that Gα13 functions as a tumor suppressor in GEM models of B cell lymphomas (Muppidi et al., 2014).

However, Gα13 loss has differential effects on the growth of Kras-expressing tumors, depending on whether there is co-expression of mutant p53. Gα13 loss in the KPC GEM model promotes tumor growth, but Gα13 is dispensable for tumor development in the KC GEM model. Instead, loss of Gα13 in the KC cell lines decreases growth in 3D collagen and in transplant models. The difference between the effects of Gα13 loss in the GEM model and the transplant models is only seen in the KC model. Although we do not know the underlying mechanism for the differential effect of Gα13 loss in the KC GEM and KC cell lines, the Maitra group found a similar effect when they expressed mutant Gαs in the context of Kras (Ideno et al., 2018). They showed that the KC cells expressing mutant Gαs show suppression of colony formation *in vitro* and a decrease in tumor growth *in vitro* (Ideno et al., 2018). This contrasts with their GEM animal data, where co-expression of mutant Gαs did not suppress tumor growth (Ideno et al., 2018).

We have found that targeting Gα13 in the KPC GEM model causes differentiated tumors. We show increased E-cadherin expression in tumors with Gα13 loss, thus explaining the well-differentiated tumors in the KPC mice with Gα13 loss. We had previously demonstrated that Gα13 loss results in increased E-cadherin at cell-cell junctions (Chow et al., 2016). Loss of Gα13 has also been shown to increase vascular endothelial (VE)-cadherin at cell-cell junctions (Gong et al., 2014). Importantly, human PDAC tumors with Gα13 loss also demonstrate increased expression of E-cadherin. However, despite the tumors being well differentiated, we show that mice with Gα13 loss in the KPC model died faster than the control KPC mice, likely from the extensive tumor burden.

We show that Gα13 loss in the KPC mouse model, but not in the KC mouse model, increases mTOR signaling and that human PDAC tumors with decreased Gα13 expression

exhibit increased mTOR signaling. We also demonstrate in human and mouse PDAC tumors with loss of Gα13 expression the activation of PDK1, which can enhance Akt/mTOR signaling (Manning and Toker, 2017). Previous studies have shown that Gα13 loss in lymphomas and osteoclasts increases Akt signaling (Muppidi et al., 2014; Wu et al., 2017), whereas overexpression of an active mutant of Gα13 in osteoclasts decreases Akt signaling (Wu et al., 2017). Importantly, we have found that the KPC tumors with Gα13 loss are susceptible to treatment with rapamycin. Notably, tumors developing in the Kras/PTEN GEM model, which exhibit increased Akt/mTOR signaling, are also susceptible to rapamycin treatment (Morran et al., 2014).

mTOR inhibitors have been evaluated in clinical trials involving pancreatic cancer patients (Javle et al., 2010; Wolpin et al., 2009). They have been tested as single agents in patients who have progressed on chemotherapy and in combination with chemotherapy. mTOR inhibitors show a lack of response as single agents or in combination with chemotherapy. However, these clinical trials in advanced pancreatic cancer were conducted in unselected patients without identifying tumors that may be particularly dependent on mTOR signaling (Javle et al., 2010; Wolpin et al., 2009). Our results suggest using the loss of Gα13 expression to select patients for studies with mTOR inhibitors.

Overall, our findings demonstrate a tumor-suppressive role of Gα13 in PDAC tumors developing in the Kras/Tp53 mouse model and suggest targeting mTOR in human PDAC tumors with Gα13 loss.

Limitations of the study

The genetic strategy we used to investigate Gα13 function in this study targets the gene *in vitro* and not in adult mice. Thus, our work does not address the effects of targeting Gα13 in adult mouse pancreas tissue with established tumors. Also, we show that Gα13 functions as a tumor suppressor in tumors with mutations in both Kras and p53 but not in tumors with only Kras mutation. It will be essential to understand how mutations in both Kras and p53 mediate the tumor-suppressive effects of Gα13. A recent report demonstrated that Gα13 could function as a tumor suppressor by its effect on the immune microenvironment (Martin et al., 2021). We have not addressed the effects of Gα13 loss on the immune microenvironment in our mouse models. Finally, while our studies demonstrate that mTOR/Rps6 signaling is activated in Gα13-deficient tumors in humans and KPC mice, the exact mechanism by which loss of Gα13 activates the mTOR/Rps6 signaling is yet to be determined.

STAR*METHODS

RESOURCE AVAILABILITY

Lead contact—Further information and request for resources and reagents should be directed to and will be fulfilled by the lead contact, Mario Shields (mario.shields@northwestern.edu>)

Materials availability—Cell lines generated in the study can be obtained through an MTA from Northwestern University.

This study did not generate other new unique reagents.

Data and code availability—This paper analyzes publicly available data from the TCGA and cBioportal databases.

The pancreatic cancer dataset from cBioportal can be access at the url: http://www.cbioportal.org/study/summary?id=paad_tcga_pan_can_atlas_2018. The specific patient samples used for comparisons are listed in Table S1.

All data reported in this paper will be shared by the lead author upon request.

This paper does not report any original code.

Any additional information required to reanalyze the data reported in this paper is available from the lead contact upon request.

EXPERIMENTAL MODELS AND SUBJECT DETAILS

Animal experiments—All animal work and procedures were approved by the Northwestern University Institutional Animal Care and Use Committee. In addition, all animal experiments were performed in accordance with relevant guidelines and regulations. The following mice were used in the study: Pdx1-Cre mice (Jackson Laboratory #014647), *Gna13* (kindly provided by Stefan Offermans, Max Planck Institute) (Moers et al., 2003), LSL-KRas$^{G12D/+}$ (Jackson Laboratory #019104) LSL-Trp53$^{R172H/+}$ (Jackson Laboratory 008652). All mice were bred on a C57/BL6 background, with ages ranging from 3–20 months and from both genders.

Animals were housed at 12h light/dark cycle in ventilated cages with controlled temperature and humidity. Water and standard mouse diet were provided ad libitum, and bedding changed regularly.

Cell lines—Cell lines used in the study were derived from autochthonous mouse pancreatic tumors. Primary cell lines from KCG$^{+/+}$ (2005, 7-month-old female; 2685, 6-month-old male), KCG$^{fl/fl}$ (1930, 9-month-old male; 1999, 10-month-old male), KPCG$^{+/+}$(2138, 3-month-old male; 3213, 3-month-old female), and KPCG$^{fl/fl}$ (3458, 5-month-old female; 3566, 4-month-old female) C57/BL6 mice were generated as described below. Cell lines were cultured in DMEM media with 10% FBS and 1% penicillin/streptomycin and at grown at 37°C with 5% CO_2 in an incubator.

METHOD DETAILS

Conditional knockout—Mice with loss of Gα13 in the pancreas were generated by crossing Pdx1-Cre mice (Jackson Laboratory #014647) to mice expressing the floxed allele of *Gna13* (kindly provided by Stefan Offermans, Max Planck Institute) (Moers et al., 2003), to generate CGα13fl/+ and CGα13fl/fl mice. The bigenic mice were further crossed with mice expressing an LSL-KRas$^{G12D/+}$ (Jackson Laboratory #019104) mutant allele to generate KCGα13fl/+ (KCGfl/+) or KCGα13fl/fl (KCGfl/fl) mice. These mice were further crossed with mice expressing LSL-Trp53$^{R172H/+}$ (Jackson Laboratory 008652) to

generate KPCGfl/+ and KPCGfl/fl mice. For survival studies, mice were aged singly or in groups of 2–5. Some mice developed anogenital or facial papillomas that were surgically removed before compromising health. Mice that developed extra-pancreatic diseases such as thymoma, prolapse, or inoperable papillomas were excluded from the study. All mice were bred on a C57/BL6 background, and both genders were used in the studies.

Cell implantation—For subcutaneous implantation, cells (2.5×10^5) were suspended in 100 μL of 1:1 mixture of PBS: Matrigel and then injected under the skin in the flank of C57BL/6 mice. After tumors were ~100 mm^3, mice were treated with vehicle control (10% PEG400, 10% Tween 80 in water) or rapamycin (MedChemExpress, HY-10219) daily at 60 mg/kg daily via intraperitoneal injections. Tumor dimensions were measured using a digital caliper, and volume was determined using the formula $V = (L \times W^2)/2$, where V is the volume, L is length, and W is the width.

Endpoint—At the experimental endpoints (tumor size, tumor ulceration, deteriorating body score, reduced weight, or moribund state), mice were euthanized. For the cell implantation studies, mice were also euthanized if the injected cells failed to form tumors or formed small tumors that grew very slowly. The pancreatic tissue or tumors were weighed and fixed in 10% neutral buffered formalin overnight or flashed frozen for RNA or protein extraction. The fixed tissue was subsequently processed and embedded in paraffin for histological stains and immunohistochemistry.

Generation of cell lines from genetically engineered mouse models—KCG+/+, KCGfl/+, or KCGfl/fl mice more than 6 months of age were euthanized, and the harvested pancreatic tissue was placed in 5 mL of cold DMEM using aseptic technique. The tissue was minced using a sterile scalpel and then placed in a 2 mg/mL Collagenase I solution diluted in DMEM and enzymatically digested at 37°C for 30 min with mixing by vortex at 10-min intervals. The digested tissue was centrifuged at 1200 rpm for 3 min, and the cell pellet was resuspended in DMEM media with 10% FBS and 1% penicillin/streptomycin. The cells were plated in a 10-cm tissue culture dish and maintained at 37°C with 5% CO_2 in an incubator. The cells were serially passaged until the culture was purely pancreatic ductal epithelial cells (at passage 4 or 5). Tumors developing in KPCG+/+, KPCGfl/+, and KPCGfl/fl were similarly processed to generate the corresponding cancer cell lines. All cells in culture were tested and confirmed to be free of mycoplasma using the Myco Alert Plus Kit (Lonza LT07–701).

3D collagen cultures—Established cell lines (5×10^3) were suspended in neutralized rat tail collagen type I (cat # 354236 Corning) at 2 mg/mL and 250 μL was dispensed in 48-well plates and maintained for 7 days (Ebine et al., 2019). The morphology of the cells growing in 3D collagen was analyzed from photographs taken using Zeiss Axiovert 40 CFL microscope and Nikon Coolpix 4500 camera. Cells were extracted out of collagen gels with collagenase (10 mg/mL, Worthington Biochem #CLS1) solution by incubating at 37°C for 20 min and single cells generated by incubating with trypsin/EDTA (0.05% Trypsin/0.53mM EDTA, Corning #25052CI) for 3–5 min. Cells were counted using trypan blue and the TC2 automated cell counter (BioRad).

Histology/Immunohistochemistry—For immunostains, paraffin-embedded sections were deparaffinized and rehydrated. Antigen retrieval was performed by boiling for 10 min in sodium citrate buffer (10 mM, pH 6.0) using a pressure cooker. Endogenous peroxidase activity in tissue was quenched, and sections were blocked with a mixture of goat serum and bovine serum albumin (BSA). Tissue sections were incubated with antibodies for: E-cadherin (Cell Signaling #3195, RRID: AB_2291471, 1:500), Cytokeratin 19 (Abcam ab52625, RRID: AB_2281020, 1:500), Ki67 (Cell Signaling #12202, RRID: AB_2620142, 1:1000), cleaved caspase-3 (Cell Signaling #9664, RRID: AB_2070042, 1:800), mTOR (Cell Signaling #2983, RRID: AB_2105622, 1:1000), p-mTOR (Abcam ab109268, RRID: AB_10888105, 1:2000), RPS6 (Cell Signaling #2217, RRID: AB_331355, 1:1000), and p-RPS6 (Cell Signaling #4858, RRID: AB_916156, 1:1000) overnight at 4°C. Antibody binding was detected using HRP-conjugated anti-rabbit secondary antibody and visualized using ImmPACT DAB Peroxidase Substrate kit (VectorLabs, Burlingame, CA). Photographs were taken on the FeinOptic microscope with a Jenoptik ProgRes C5 camera or TissueGnostics system and analyzed by Aperio Software. Trichrome and hematoxylin and eosin (H&E) stains were routinely conducted by the Lurie Cancer Center Pathology Core.

Immunofluorescence—Antigen retrieval was performed similarly to the immunohistochemistry procedure above. Tissue sections were blocked with a mixture of goat serum and bovine serum albumin for 1 h. Tissue sections were incubated with a mixture of antibodies for CK19 (DSHB TROMA-III, RRID: AB_2133570,1:100) and Ki67 (Cell Signaling #12202, RRID: AB_2620142, 1:500) for 2 h at room temperature. After washing, tissue sections were incubated with a mixture of goat anti-rat Alexa Fluor 594 (ThermoFisher, RRID: AB_10561522 #A-11007, 1:200) and goat anti-rabbit AlexaFluor 488Plus (ThermoFisher #A-32731, RRID: AB_2633280 1:200) secondary antibodies and protected from light. Sections were incubated with DAPI (#D1306 ThermoFisher) for nuclear counterstain and mounted in fluorescence mounting media (#S302380, Agilent). Images were acquired with the EVOS M5000 (ThermoFisher) fluorescence microscope using a 40X lens. At least 10 sections were acquired per tissue section, and ImageJ was used to analyze the double-positive CK19 and Ki67 areas.

Western blot—Tissue samples were finely ground using a cold mortar and pestle or the Minilys bead-based homogenizer (#P000673-MYLS0-A, Bertin Corp. with ceramic beads (#CK28, Bertin Corp). Protein was isolated from cultured cells or ground tissue using ice-cold RIPA lysis buffer containing protease and phosphatase inhibitors. The lysates were then clarified by centrifugation at 10,000 rpm for 10 min at 4°C, and the protein concentration was determined using Precision Red solution (#ADV02, Cytoskeleton, Inc., Denver, CO) according to the manufacturer's instructions. Equal amounts of protein were separated with a 10% or 6% SDS-PAGE electrophoresis gel. The separated proteins were transferred to a PVDF (#IPVH00010, Millipore Sigma) membrane using the semi-dry transfer system (Bio-Rad). After blocking for one hour at room temperature with 5% BSA, the membranes were incubated overnight at 4°C with primary antibodies. Primary antibodies used include Gα13 (Santa Cruz #sc-293424, 1:1,000), E-cadherin (Cell Signaling #3195, RRID:AB_2291471, 1: 5,000), PDK1 (Cell Signaling #5662, AB_10839264, 1:1,000), p-PDK1 (Cell Signaling #3438, RRID:AB_2161134 1:1,000) mTOR (Cell Signaling #2983, RRID: AB_2105622,

1:1,000), p-mTOR(Abcam ab109268, RRID: AB_10888105, 1:1,000), RPS6(Cell Signaling #2217, RRID:AB_331355, 1:10,000), p-RPS6 (Cell Signaling #4858, RRID: AB_916156, 1:10,000), Gapdh (Millipore Sigma #MAB374, RRID: AB_2107445 1:5,000), and Hsp90 (Santa Cruz Biotechnology sc-7947, RRID: AB_2121235 1:5,000). HRP-conjugated rabbit (#A6667, RRID: AB_258307, 1:10,000) or mouse (#A4416, RRID: AB_258167, 1:10,000) secondary antibody (Millipore-Sigma St. Louis, MO) was used with SuperSignal West Pico PLUS (Thermo Fisher Scientific) for protein detection.

qRT-PCR—RNA was isolated from cultured cells or tissue using the RNeasy kit (74104, QIAGEN, Hilden, Germany) according to the manufacturer's instructions. cDNA was synthesized from 1–2 μg of RNA with random hexamers and M-MLV reverse transcriptase in a single 50 μL reaction. Quantitative PCR was performed using *Gna13* (Mm01250415_m1) and *Gapdh* (Mm99999915_g1) TaqMan probes, TaqMan Universal PCR Master Mix, and the CFX Connect Real-Time PCR Detection System (Bio-Rad Hercules, CA). The relative expression was calculated using the comparative Ct method (Livak and Schmittgen, 2001).

TCGA data analysis—Expression data from RNA and protein (RPPA) analyses for human pancreatic ductal adenocarcinoma patients in The Cancer Genome Atlas (TCGA) were extracted from cBioportal (Cerami et al., 2012; Gao et al., 2013). Patient IDs from the study are listed in Table S1 and are categorized as high (GNA13 hi, upper 25%, n = 43) or low (GNA13 lo, lower 25%, n = 43) expression of *GNA13* RNA.

QUANTIFICATION AND STATISTICAL ANALYSIS

The *in vivo* and *in vitro* results were compared using one-way ANOVA with Bonferroni correction and 2-tailed t test analysis. Error bars represent the standard error of the mean or standard deviation as specified in the figure legends. All statistical analyses were done using GraphPad Prism. Statistical details of experiments can be found in the figure legends or method details including the statistical tests used, number (n) of tumors, animals or cells. For all analyses error bar represent standard deviation except where noted. A p value of less than 0.05 was considered significant.

Supplementary Material

Refer to Web version on PubMed Central for supplementary material.

ACKNOWLEDGMENTS

REFERENCES

Cerami E, Gao J, Dogrusoz U, Gross BE, Sumer SO, Aksoy BA, Jacobsen A, Byrne CJ, Heuer ML, Larsson E, et al. (2012). The cBio cancer genomics portal: an open platform for exploring multidimensional cancer genomics data. Cancer Discov. 2, 401–404. 10.1158/2159-8290.CD-12-0095. [PubMed: 22588877]

Chow CR, Ebine K, Knab LM, Bentrem DJ, Kumar K, and Munshi HG (2016). Cancer cell invasion in three-dimensional collagen is regulated differentially by Galpha13 protein and discoidin domain receptor 1-Par3 protein signaling. J. Biol. Chem. 291, 1605–1618. 10.1074/jbc.M115.669606. [PubMed: 26589794]

Ebine K, Chow CR, and Munshi HG (2019). Quantitative method to track proteolytic invasion in 3D collagen. Methods Mol. Biol. 1882, 161–169. 10.1007/978-1-4939-8879-2_15. [PubMed: 30378053]

Farrell JJ, and Fernandez-del Castillo C (2013). Pancreatic cystic neoplasms: management and unanswered questions. Gastroenterology 144, 1303–1315. 10.1053/j.gastro.2013.01.073. [PubMed: 23622140]

Gao J, Aksoy BA, Dogrusoz U, Dresdner G, Gross B, Sumer SO, Sun Y, Jacobsen A, Sinha R, Larsson E, et al. (2013). Integrative analysis of complex cancer genomics and clinical profiles using the cBioPortal. Sci. Signal 6, pl1. 10.1126/scisignal.2004088. [PubMed: 23550210]

Gong H, Gao X, Feng S, Siddiqui MR, Garcia A, Bonini MG, Komarova Y, Vogel SM, Mehta D, and Malik AB (2014). Evidence of a common mechanism of disassembly of adherens junctions through Galpha13 targeting of VE-cadherin. J. Exp. Med. 211, 579–591. 10.1084/jem.20131190. [PubMed: 24590762]

Hauser AS, Attwood MM, Rask-Andersen M, Schioth HB, and Gloriam DE (2017). Trends in GPCR drug discovery: new agents, targets and indications. Nat. Rev. Drug Discov. 16, 829–842. 10.1038/nrd.2017.178. [PubMed: 29075003]

Healy JA, Nugent A, Rempel RE, Moffitt AB, Davis NS, Jiang X, Shingleton JR, Zhang J, Love C, Datta J, et al. (2016). GNA13 loss in germinal center B cells leads to impaired apoptosis and promotes lymphoma *in vivo*. Blood 127, 2723–2731. 10.1182/blood-2015-07-659938. [PubMed: 26989201]

Hingorani SR, Petricoin EF, Maitra A, Rajapakse V, King C, Jacobetz MA, Ross S, Conrads TP, Veenstra TD, Hitt BA, et al. (2003). Preinvasive and invasive ductal pancreatic cancer and its early detection in the mouse. Cancer cell 4, 437–450. [PubMed: 14706336]

Hingorani SR, Wang L, Multani AS, Combs C, Deramaudt TB, Hruban RH, Rustgi AK, Chang S, and Tuveson DA (2005). Trp53R172H and KrasG12D cooperate to promote chromosomal instability and widely metastatic pancreatic ductal adenocarcinoma in mice. Cancer cell 7, 469–483. [PubMed: 15894267]

Ideno N, Yamaguchi H, Ghosh B, Gupta S, Okumura T, Steffen DJ, Fisher CG, Wood LD, Singhi AD, Nakamura M, et al. (2018). GNAS(R201C) induces pancreatic cystic neoplasms in mice that express activated KRAS by inhibiting YAP1 signaling. Gastroenterology 155, 1593–1607. 10.1053/j.gastro.2018.08.006. [PubMed: 30142336]

Javle MM, Shroff RT, Xiong H, Varadhachary GA, Fogelman D, Reddy SA, Davis D, Zhang Y, Wolff RA, and Abbruzzese JL (2010). Inhibition of the mammalian target of rapamycin (mTOR) in advanced pancreatic cancer: results of two phase II studies. BMC Cancer 10, 368. 10.1186/1471-2407-10-368. [PubMed: 20630061]

Kelly P, Casey PJ, and Meigs TE (2007). Biologic functions of the G12 subfamily of heterotrimeric g proteins: growth, migration, and metastasis. Biochemistry 46, 6677–6687. 10.1021/bi700235f. [PubMed: 17503779]

Kelly P, Moeller BJ, Juneja J, Booden MA, Der CJ, Daaka Y, Dewhirst MW, Fields TA, and Casey PJ (2006). The G12 family of heterotrimeric G proteins promotes breast cancer invasion and metastasis. Proc. Natl. Acad. Sci. U S A 103, 8173–8178. 10.1073/pnas.0510254103. [PubMed: 16705036]

Kozasa T, Hajicek N, Chow CR, and Suzuki N (2011). Signalling mechanisms of RhoGTPase regulation by the heterotrimeric G proteins G12 and G13. J. Biochem. 150, 357–369. 10.1093/jb/mvr105. [PubMed: 21873336]

Kurose H (2003). Galpha12 and Galpha13 as key regulatory mediator in signal transduction. Life Sci. 74, 155–161. 10.1016/j.lfs.2003.09.003. [PubMed: 14607242]

Livak KJ, and Schmittgen TD (2001). Analysis of relative gene expression data using real-time quantitative PCR and the 2(-Delta Delta C(T)) Method. Methods 25, 402–408. 10.1006/meth.2001.1262. [PubMed: 11846609]

Lowy AM, Fenoglio-Preiser C, Kim OJ, Kordich J, Gomez A, Knight J, James L, and Groden J (2003). Dysregulation of beta-catenin expression correlates with tumor differentiation in pancreatic duct adenocarcinoma. Ann. Surg. Oncol. 10, 284–290. 10.1245/aso.2003.05.003. [PubMed: 12679314]

Manning BD, and Toker A (2017). AKT/PKB signaling: navigating the network. Cell 169, 381–405. 10.1016/j.cell.2017.04.001. [PubMed: 28431241]

Martin TD, Patel RS, Cook DR, Choi MY, Patil A, Liang AC, Li MZ, Haigis KM, and Elledge SJ (2021). The adaptive immune system is a major driver of selection for tumor suppressor gene inactivation. Science 373, 1327–1335. 10.1126/science.abg5784. [PubMed: 34529489]

Matthaei H, Schulick RD, Hruban RH, and Maitra A (2011). Cystic precursors to invasive pancreatic cancer. Nat. Rev. Gastroenterol. Hepatol. 8, 141–150. 10.1038/nrgastro.2011.2. [PubMed: 21383670]

Maziarz M, Federico A, Zhao J, Dujmusic L, Zhao Z, Monti S, Varelas X, and Garcia-Marcos M (2020). Naturally occurring hotspot cancer mutations in Galpha13 promote oncogenic signaling. J. Biol. Chem. 295, 16897–16904. 10.1074/jbc.AC120.014698. [PubMed: 33109615]

Moers A, Nieswandt B, Massberg S, Wettschureck N, Gruner S, Konrad I, Schulte V, Aktas B, Gratacap MP, Simon MI, et al. (2003). G13 is an essential mediator of platelet activation in hemostasis and thrombosis. Nat. Med. 9, 1418–1422. 10.1038/nm943. [PubMed: 14528298]

Molin MD, Matthaei H, Wu J, Blackford A, Debeljak M, Rezaee N, Wolfgang CL, Butturini G, Salvia R, Bassi C, et al. (2013). Clinicopathological correlates of activating GNAS mutations in intraductal papillary mucinous neoplasm (IPMN) of the pancreas. Ann. Surg. Oncol. 20, 3802–3808. 10.1245/s10434-013-3096-1. [PubMed: 23846778]

Morran DC, Wu J, Jamieson NB, Mrowinska A, Kalna G, Karim SA, Au AY, Scarlett CJ, Chang DK, Pajak MZ, et al. (2014). Targeting mTOR dependency in pancreatic cancer. Gut 63, 1481–1489. https://doi. org/10.1136/gutjnl-2013–306202. [PubMed: 24717934]

Muppidi JR, Schmitz R, Green JA, Xiao W, Larsen AB, Braun SE, An J, Xu Y, Rosenwald A, Ott G, et al. (2014). Loss of signalling via Galpha13 in germinal centre B-cell-derived lymphoma. Nature 516, 254–258. 10.1038/nature13765. [PubMed: 25274307]

O'Hayre M, Inoue A, Kufareva I, Wang Z, Mikelis CM, Drummond RA, Avino S, Finkel K, Kalim KW, DiPasquale G, et al. (2016). Inactivating mutations in GNA13 and RHOA in Burkitt's lymphoma and diffuse large B-cell lymphoma: a tumor suppressor function for the Galpha13/RhoA axis in B cells. Oncogene 35, 3771–3780. 10.1038/onc.2015.442. [PubMed: 26616858]

Oldham WM, and Hamm HE (2008). Heterotrimeric G protein activation by G-protein-coupled receptors. Nat. Rev. Mol. Cell Biol. 9, 60–71. https://doi. org/10.1038/nrm2299. [PubMed: 18043707]

Patra KC, Kato Y, Mizukami Y, Widholz S, Boukhali M, Revenco I, Grossman EA, Ji F, Sadreyev RI, Liss AS, et al. (2018). Mutant GNAS drives pancreatic tumourigenesis by inducing PKA-mediated SIK suppression and reprogramming lipid metabolism. Nat. Cell Biol. 20, 811–822. https://doi. org/10.1038/s41556–018-0122–3. [PubMed: 29941929]

Pham TND, Shields MA, Spaulding C, Principe DR, Li B, Underwood PW, Trevino JG, Bentrem DJ, and Munshi HG (2021). Preclinical models of pancreatic ductal adenocarcinoma and their utility in immunotherapy studies. Cancers (Basel) 13, 440. 10.3390/cancers13030440. [PubMed: 33503832]

Rasheed SAK, Leong HS, Lakshmanan M, Raju A, Dadlani D, Chong FT, Shannon NB, Rajarethinam R, Skanthakumar T, Tan EY, et al. (2018). GNA13 expression promotes drug resistance and tumor-initiating phenotypes in squamous cell cancers. Oncogene 37, 1340–1353. 10.1038/s41388-017-0038-6. [PubMed: 29255247]

Soini Y, Takasawa A, Eskelinen M, Juvonen P, Karja V, Hasegawa T, Murata M, Tanaka S, Kojima T, and Sawada N (2012). Expression of claudins 7 and 18 in pancreatic ductal

adenocarcinoma: association with features of differentiation. J. Clin. Pathol. 65, 431–436. 10.1136/jclin-path-2011-200400. [PubMed: 22396552]

Sriram K, Salmeron CS, Wiley SZ, and Insel PA (2020). GPCRs in pancreatic adenocarcinoma: contributors to tumor biology and novel therapeutic targets. Br. J. Pharmacol. 177, 2434–2455. 10.1111/bph.15028. [PubMed: 32060895]

Syrovatkina V, Alegre KO, Dey R, and Huang XY (2016). Regulation, signaling, and physiological functions of G-proteins. J. Mol. Biol. 428, 3850–3868. 10.1016/j.jmb.2016.08.002. [PubMed: 27515397]

Syrovatkina V, and Huang XY (2019). Signaling mechanisms and physiological functions of G-protein Galpha13 in blood vessel formation, bone homeostasis, and cancer. Protein Sci. 28, 305–312. 10.1002/pro.3531. [PubMed: 30345641]

Taki K, Ohmuraya M, Tanji E, Komatsu H, Hashimoto D, Semba K, Araki K, Kawaguchi Y, Baba H, and Furukawa T (2016). GNAS(R201H) and Kras(G12D) cooperate to promote murine pancreatic tumorigenesis recapitulating human intraductal papillary mucinous neoplasm. Oncogene 35, 2407–2412. 10.1038/onc.2015.294. [PubMed: 26257060]

Tutunea-Fatan E, Lee JC, Denker BM, and Gunaratnam L (2020). Heterotrimeric Galpha12/13 proteins in kidney injury and disease. Am. J. Physiol. Ren. Physiol 318, F660–F672. 10.1152/ajprenal.00453.2019.

Voyno-Yasenetskaya TA, Pace AM, and Bourne HR (1994). Mutant alpha subunits of G12 and G13 proteins induce neoplastic transformation of Rat-1 fibroblasts. Oncogene 9, 2559–2565. [PubMed: 8058319]

Wolpin BM, Hezel AF, Abrams T, Blaszkowsky LS, Meyerhardt JA, Chan JA, Enzinger PC, Allen B, Clark JW, Ryan DP, and Fuchs CS (2009). Oral mTOR inhibitor everolimus in patients with gemcitabine-refractory metastatic pancreatic cancer. J. Clin. Oncol. 27, 193–198. 10.1200/JCO.2008.18.9514. [PubMed: 19047305]

Wu J, Matthaei H, Maitra A, Dal Molin M, Wood LD, Eshleman JR, Goggins M, Canto MI, Schulick RD, Edil BH, et al. (2011). Recurrent GNAS mutations define an unexpected pathway for pancreatic cyst development. Sci. Transl Med. 3, 92ra66. 10.1126/scitranslmed.3002543.

Wu M, Chen W, Lu Y, Zhu G, Hao L, and Li YP (2017). Galpha13 negatively controls osteoclastogenesis through inhibition of the Akt-GSK3beta-NFATc1 signalling pathway. Nat. Commun. 8, 13700. 10.1038/ncomms13700. [PubMed: 28102206]

Xu N, Voyno-Yasenetskaya T, and Gutkind JS (1994). Potent transforming activity of the G13 alpha subunit defines a novel family of oncogenes. Biochem. Biophys. Res. Commun. 201, 603–609. 10.1006/bbrc.1994.1744.

Zhang Z, Tan X, Luo J, Cui B, Lei S, Si Z, Shen L, and Yao H (2018). GNA13 promotes tumor growth and angiogenesis by upregulating CXC chemokines via the NF-kappaB signaling pathway in colorectal cancer cells. Cancer Med. 7, 5611–5620. 10.1002/cam4.1783. [PubMed: 30267476]

Highlights

- Loss of Gα13 in the KPC GEM model promotes pancreatic tumor development

- Tumors from KPC mice with Gα13 loss demonstrate increased E-cadherin expression

- Human pancreatic tumors with reduced Gα13 expression exhibit increased mTOR signaling

- Gα13 loss sensitizes KPC tumors to rapamycin and reduces tumor growth *in vivo*
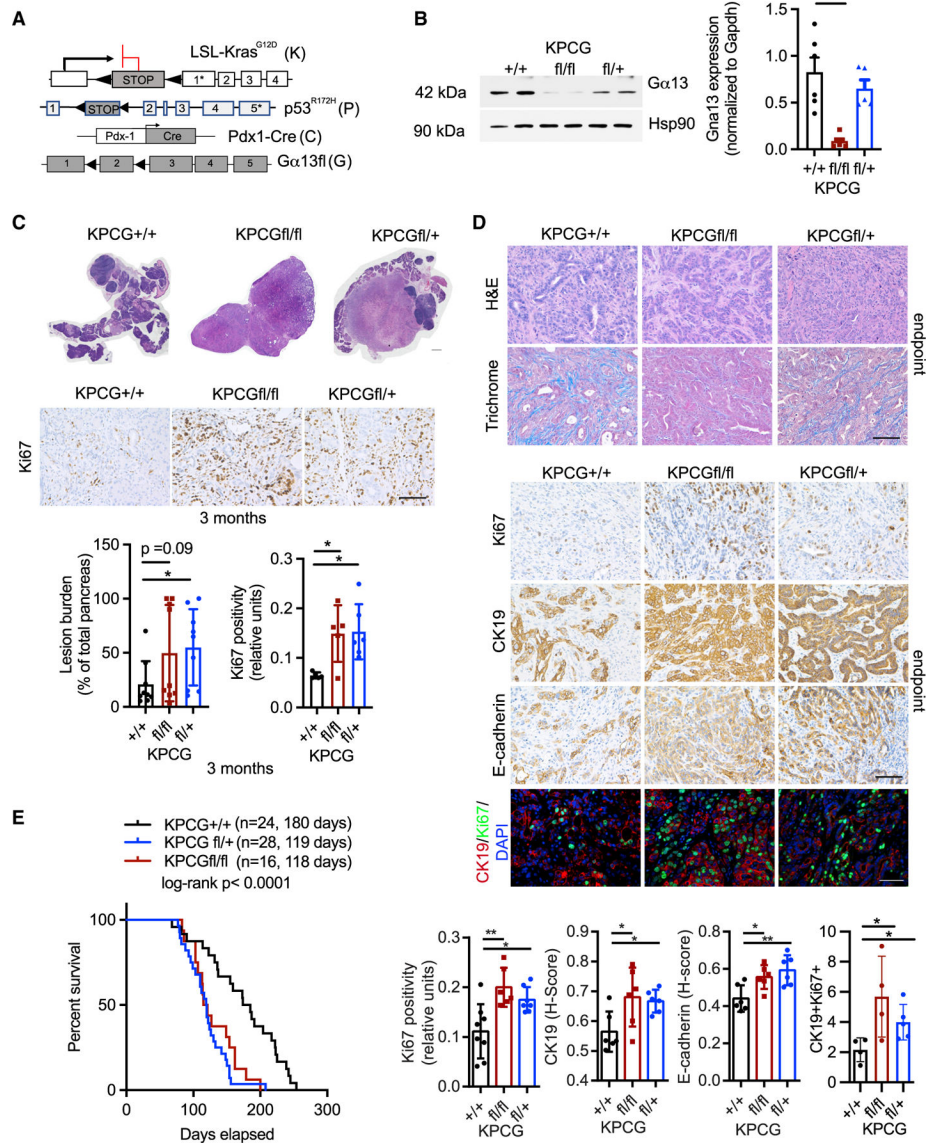
Figure 1. Loss of Gα13 in the KPC GEM model promotes pancreatic tumor development and progression

(A) Alleles of Kras^{G12D} (K), Trp53^{R172H} (P), Pdx1-Cre (C), and Gα13fl (G).

(B) Gα13 expression levels in the pancreas of mice of indicated genotypes were determined by western blotting. Heat shock protein (Hsp90) was used as an endogenous control. The expression of Gna13 was determined by qRT-PCR. GAPDH was used as an endogenous control. One-way ANOVA (n = 6 for KPCG$^{+/+}$, n = 6 for KPCG$^{fl/fl}$, and n = 5 for KPCG$^{fl/+}$ genotype). ***p   0.001, mean ± SD.

(C) The whole profile of pancreas tissue from KPCG$^{+/+}$, KPCG$^{fl/fl}$, and KPCG$^{fl/+}$ mice at 3 months was scanned, and the relative lesion burden was quantified (n = 9, 9, and 9, respectively). One-way ANOVA, * p   0.05, mean ± SD. Scale bar = 1 mm (H&E), 100 μm (IHC). Ki67 (n = 5, 5, and 5, respectively) stains of the pancreatic tissue from KPCG$^{+/+}$, KPCG$^{fl/fl}$, and KPCG$^{fl/+}$ mice at 3 months.

(D), H&E, trichrome, Ki67 (n = 8, 6, 7), CK19 (n = 6, 6, 6), and E-cadherin (n = 6, 6, 6) stains of the pancreatic tissue from KPCG$^{+/+}$, KPCG$^{fl/fl}$, and KPCG$^{fl/+}$ mice at the survival endpoints. One-way ANOVA, * p   0.05, ** p   0.01, mean ± SD. Scale bar = 100 μm. Immunofluorescence co-staining of CK19 and Ki67 of pancreatic tissue from KPCG$^{+/+}$ (n = 4), KPCG$^{fl/fl}$ (n = 4), and KPCG$^{fl/+}$ (n = 4) mice at the survival endpoint, and the double-positive (CK19^{+}/Ki67^{+}) cells were quantified. Scale bar = 50 μm. One-way ANOVA, * p   0.05, mean ± SD.

(E) Kaplan-Meier survival analysis of KPCG$^{+/+}$ (n = 24), KPCG$^{fl/+}$ (n = 28), and KPCG$^{fl/fl}$ (n = 16) mice using log-rank test.
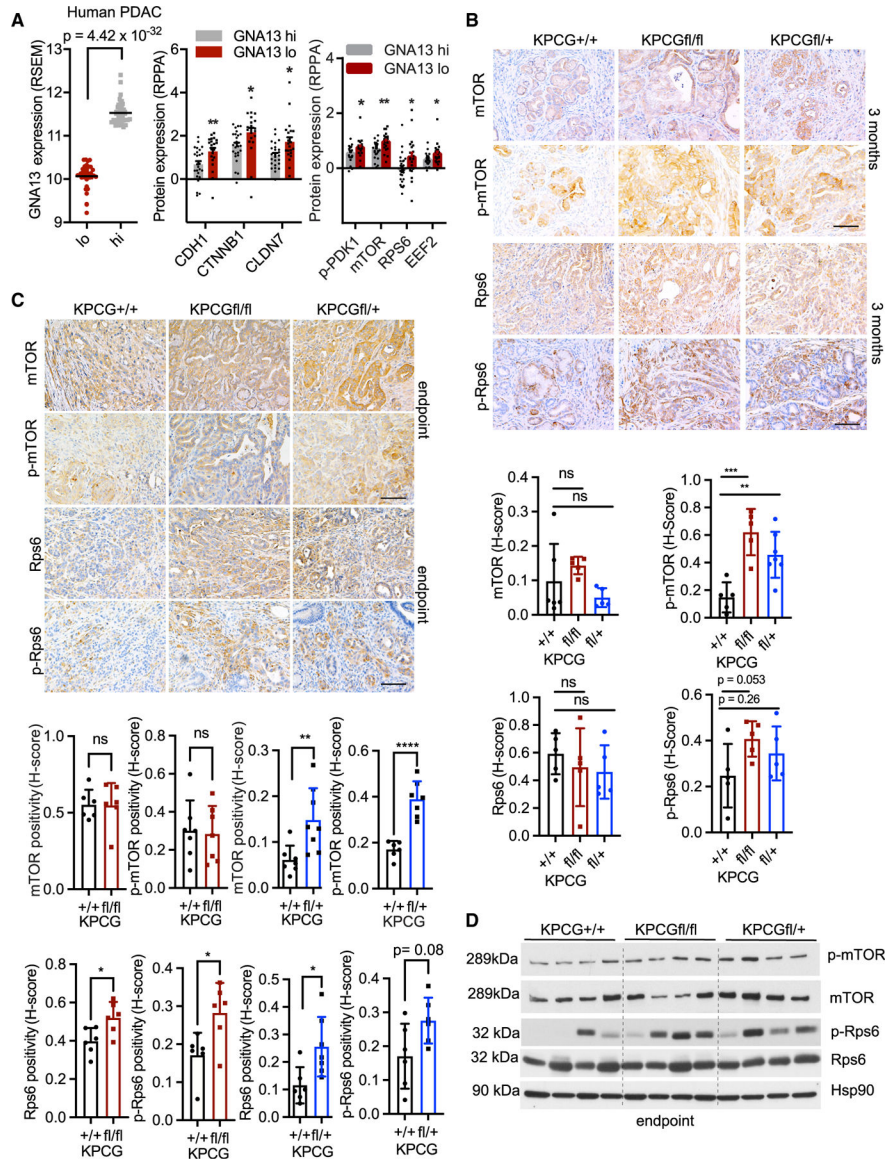
Figure 2. Human PDAC tumors with reduced Gα13 expression and tumors developing in the KPCG^{fl/fl} and KPCG^{fl/+} mice demonstrate increased mTOR signaling

(A) Analysis of samples in cBioPortal with low and high expression of *GNA13* for E-cadherin (CDH1), catenin-β1 (CTNNB1), claudin-7 (CLDN7), p-PDK1 (p-S241), mTOR, RPS6, and EEF2 at the protein level using the reverse-phase protein array (RPPA) data (n = 43 and 43, respectively). t test, mean ± SEM,*p ≤ 0.05, **p ≤ 0.01.

(B) Immunostains and quantification for mTOR (n = 6, 5, and 5, respectively), p-mTOR (n = 5, 5, and 7, respectively), Rps6 (n = 5, 5, and 5, respectively), and p-Rps6 (n = 5, 5, and 5, respectively) in lesions developing in the KPCG^{+/+}, KPCG^{fl/fl}, and KPCG^{fl/+} mice at 3 months. One-way ANOVA, mean ± SD. Scale bar = 100 μm. **p ≤ 0.01, ***p ≤ 0.001.

(C) Immunostains and quantification for mTOR (n = 6, 6, and 8, respectively), p-mTOR (n = 6, 7, and 7, respectively), Rps6 (n = 6, 6, and 7, respectively), and p-Rps6 (n = 6, 6, and 6, respectively) in tumors developing in the KPCG^{+/+}, KPCG^{fl/fl}, and KPCG^{fl/+} mice at

survival endpoints. t test, mean ± SD. Scale bar = 100 μm. *p   0.05, **p   0.01, ****p 0.0001.

(D) Western blot analysis of tumor lysates from KPCG^{+/+}, KPCG^{fl/fl}, and KPCG^{fl/+} mice for p-mTOR, mTOR, p-Rps6, and Rps6 at survival endpoints.
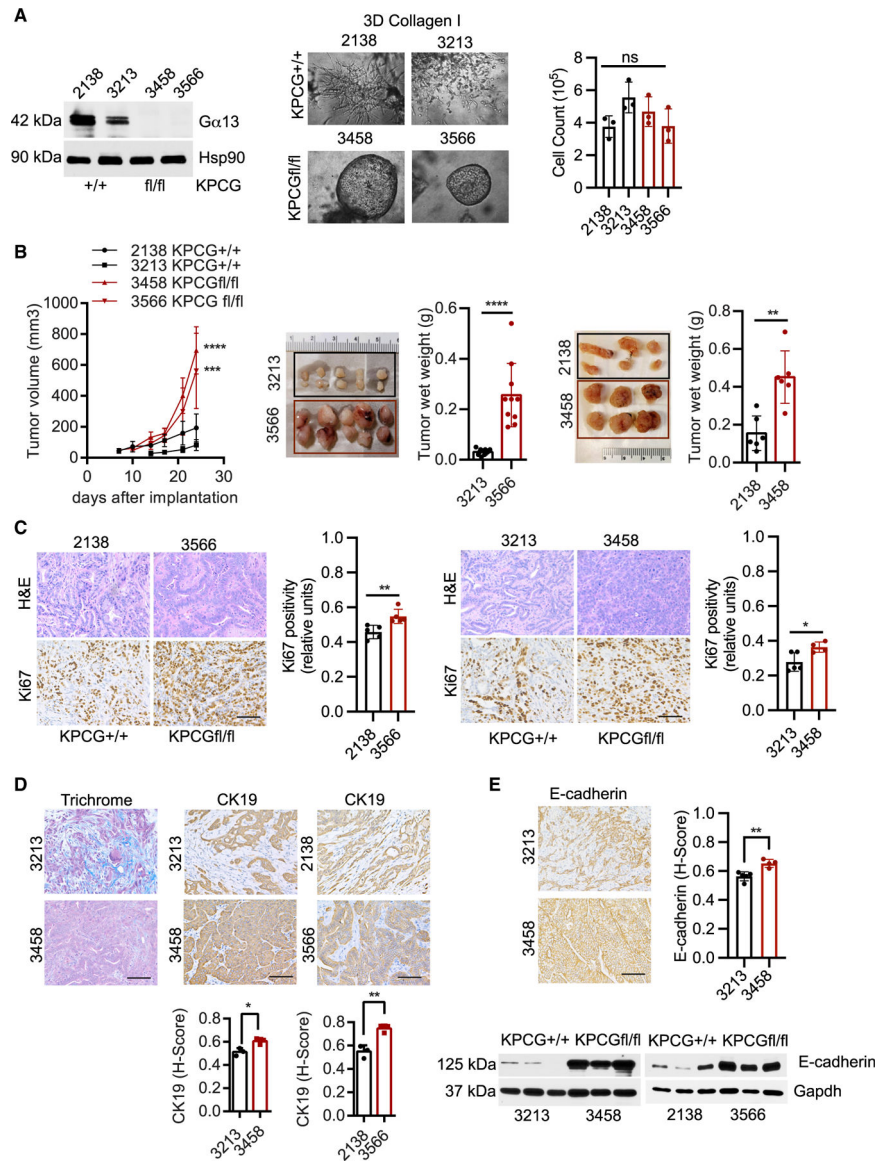
Figure 3. Cell lines established from KPCG^{fl/fl} mice demonstrate increased tumor growth with increased E-cadherin expression

(A) Western blot for Gα13 in pancreatic cancer cell lines established from tumors developing in KPCG^{+/+} (2138 and 3213) and KPCG^{fl/fl} (3458 and 3566) mice. Equal numbers of 2138, 3213, 3458, and 3566 cells were grown in 3D type I collagen, and pictures were taken after 5 days. The cells were extracted out of collagen and counted. This experiment was repeated at least 3 times.

(B) The cells were implanted subcutaneously in the flank of B6 mice (6–8 weeks old). The tumor sizes were measured using a caliper, harvested day ~24, and photographed, and wet weight was measured (2138 n = 3, 3213 n = 5, 3458 n = 3, and 3566 n = 5 mice; 2 tumors per mouse). One-way ANOVA for tumor growth, mean ± SD, ***p   0.001, ****p 0.0001. t test, mean ± SD for tumor weights. **p   0.01, ****p   0.0001.

(C) H&E and immunostains and quantification of Ki67 in the KPCG^{+/+} and KPCG^{fl/fl} tumors. t test, mean ± SD. Scale bar = 100 μm. *p   0.05, **p   0.01

(D and E) Trichrome, CK-19, and E-cadherin stains of tumors developing in the KPCG$^{+/+}$ and KPCG$^{fl/fl}$ mice. t test, mean ± SD. Scale bar = 100 μm. *p   0.05, **p   0.01. The tumors were also analyzed for E-cadherin expression by western blotting.
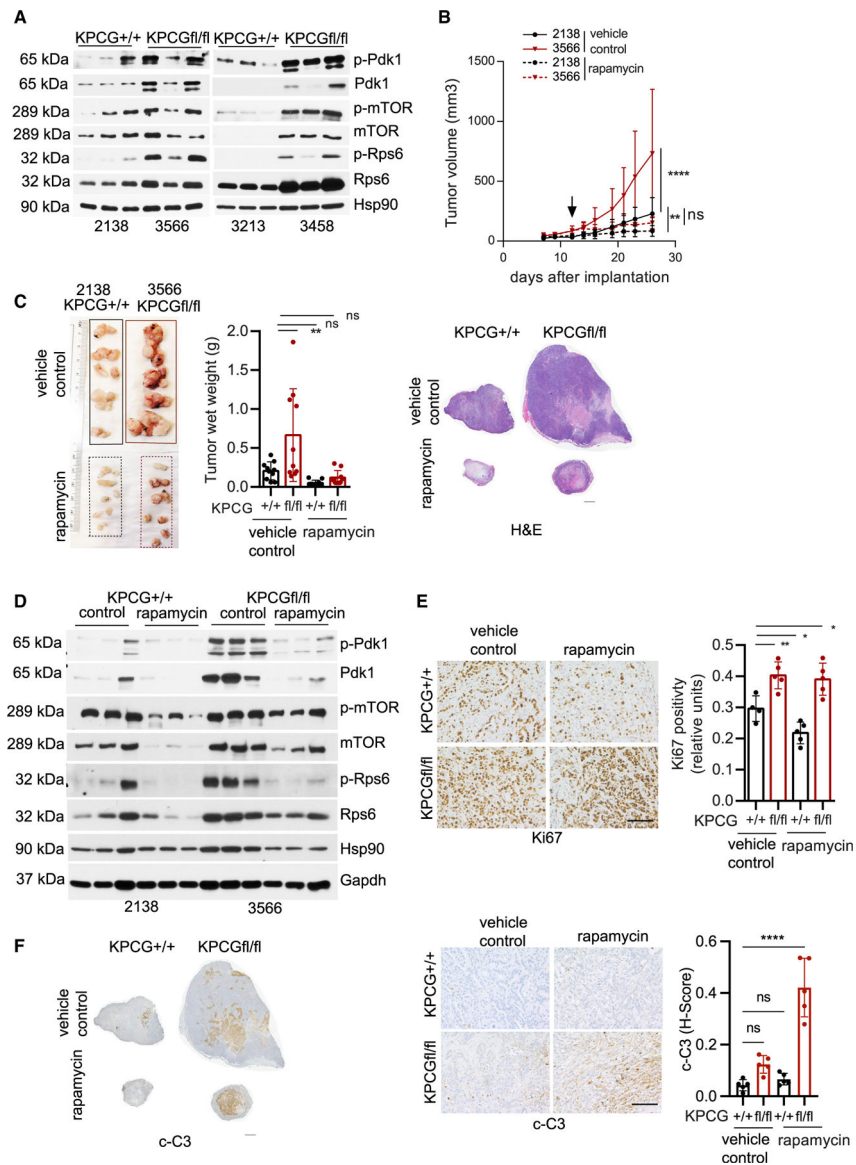
Figure 4. Gα13 loss sensitizes KPC tumors to the mTOR inhibitor rapamycin and reduces tumor growth *in vivo*

(A) Syngeneic KPCG$^{+/+}$ and KPCG$^{fl/fl}$ tumors were analyzed for p-Pdk1, Pdk1, p-mTOR, mTOR, p-Rps6, and Rps6 by western blotting using Hsp90 as a loading control.

(B and C) The KPCG$^{+/+}$ and KPCG$^{fl/fl}$ cells were implanted subcutaneously in the flank of B6 mice (6–8 weeks old) and treated with vehicle control or rapamycin (60 mg/kg daily; arrow indicates the start of treatment), once the tumors reached ~100 mm^3. The tumor sizes were measured using a caliper, harvested day 27, and photographed, and wet weight was measured. (n = 5 mice per group; 2 tumors per mouse). Representative whole profile of H&E stains of vehicle control and rapamycin-treated tumors. One-way ANOVA, mean ± SD. **p 0.01, ****p 0.0001.

(D) Tumors treated with vehicle control or rapamycin were analyzed for p-Pdk1, Pdk1, p-mTOR, mTOR, p-Rps6, and Rps6 by western blotting using Hsp90/GAPDH as loading controls.

(E) The effect of rapamycin on proliferation was analyzed by immunostains and quantification of Ki67 in the KPCG$^{+/+}$ and KPCG$^{fl/fl}$ tumors. One-way ANOVA (n = vehicle control KPCG$^{+/+}$ and KPCG$^{fl/fl}$ [4 and 5], rapamycin KPCG$^{+/+}$ and KPCG$^{fl/fl}$ [5 and 5]), t test, mean ± SD. Scale bar = 100 μm. *p ≤ 0.05, **p ≤ 0.01.

(F) Whole profile of cleaved-caspase 3 (c-C3) stains of vehicle control and rapamycin-treated tumors. Higher magnification and quantification of c-C3 stains in the treated tumors. One-way ANOVA (n = 5, 5, 5, and 5, per treatment group). ****p < 0.0001.

KEY RESOURCES TABLE

REAGENT or RESOURCE	SOURCE	IDENTIFIER
Antibodies		
E-Cadherin (24E10)	Cell Signaling	Cat# 3195; RRID:AB_2291471
Cytokeratin 19	Developmental Studies Hybridoma Bank (DSHB)	Cat# TROMA-III; RRID:AB_2133570
Cytokeratin 19 (EP1580Y)	Abcam	Cat# ab52625; RRID:AB_2281020
Ki67 (D3B5)	Cell Signaling	Cat 12202; RRID:AB_2620142
Cleaved caspase 3 (5A1E)	Cell Signaling	Cat# 9664; RRID:AB_2070042
mTOR (7C10)	Cell Signaling	Cat 2983; RRID:AB_2105622
Phosphorylated-mTOR (EPR426(2))	Abcam	Cat# ab109268; RRID:AB_10888105
RPS6 (5G10)	Cell Signaling	Cat# 2217; RRID:AB_331355
Phosphorylated-RPS6 (D57.2.2E)	Cell Signaling	Cat# 4858; RRID:AB_916156
PDK1 (D37A7)	Cell Signaling	Cat# 5662; RRID:AB_10839264
Phosphorylated-PDK1 (C49H2)	Cell Signaling	Cat# 3438; RRID:AB_2161134
Gα13 (6F6-B5)	Santa Cruz Biotech	Cat# sc-293424
HSP90 (H114)	Santa Cruz Biotech	Cat# sc-7947; RRID:AB_2121235
GAPDH (6C5)	Sigma Millipore	Cat# MAB374; RRID:AB_2107445
HRP-conjugated anti-rabbit	Sigma Millipore	Cat# A6667; RRID:AB_258307
HRP-conjugated anti-mouse	Sigma Millipore	Cat# A4416; RRID:AB_258167
Alexa Fluor 594-Conjugated goat anti-rat	Thermo Fisher	Cat# A-11007; RRID:AB_10561522
AlexaFluor 488Plus-Conjugated goat anti-rabbit	Thermo Fisher	Cat# A32731; RRID:AB_2633280
Chemicals, peptides, and recombinant proteins		
Collagenase I	Worthington Biochem	Cat# CLS1
Rapamycin	MedChem Express	Cat# HY-10219
Rat tail collagen type I	Corning	Cat# 354236
Trypsin/EDTA	Corning	Cat# 25052CI
PEG 400	MedChem Express	Cat# HY-Y0873A
Tween 80	Sigma Millipore	Cat# P8074
Reduced Growth Factor Basement Membrane Extract (Cultrex)	R&D Systems	Cat# 3433-005-01
Critical commercial assays		
RNeasy kit	Qiagen	Cat# 74104
TaqMan Reverse Transcription reagents	Thermo Fisher	Cat# N080234
TaqMan Universal PCR Master Mix	Thermo Fisher	Cat# 4324018
ImmPACT DAB Peroxidase Substrate kit	Vector Labs	Cat# SK-4105
Precision Red protein assay reagent	Cytoskeleton	Cat# ADV02
SuperSignal West Pico Plus	Thermo Fisher	Cat# 34580
Myco Alert Plus Kit	Lonza	Cat# LT07-701

REAGENT or RESOURCE	SOURCE	IDENTIFIER
Deposited data		
TCGA	cBioportal	http://www.cbioportal.org/study/summary?id=paad_tcga_pan_can_atlas_2018
Experimental models: Cell lines		
1930	This paper	N/A
1999	This paper	N/A
2005	This paper	N/A
2685	This paper	N/A
2138	This paper	N/A
3213	This paper	N/A
3458	This paper	N/A
3566	This paper	N/A
Experimental models: Organisms/strains		
Mouse: Pdx1-Cre	Jackson Laboratory	RRID:IMSR_JAX:014647
Mouse: LSL-Trp53$^{R172H/+}$	Jackson Laboratory	RRID:IMSR_JAX:008652
Mouse: Kras$^{G12D/+}$	Jackson Laboratory	RRID:IMSR_JAX:019104
Mouse: Gα13^{fl}	Stefan Offermans, MPI	RRID:MGI:3697690
Oligonucleotides		
Gna13 Taqman probe	Thermo Fisher	Mm01250415_m1
Gapdh Taqman probe	Thermo Fisher	Mm99999915_g1
Software and algorithms		
GraphPad Prism	GraphPad http://www.graphpad.com/	V 9.2.0 RRID:SCR_002798
TissueGnostics, TissueFAXS	TissueGnostics https://tissuegnostics.com	V 7.0 RRID:SCR_020996
Fiji ImageJ2	https://fiji.sc	V 2.3.0 RRID:SCR_002285
Aperio ImageScope	Leica	V 12.3.3 RRID:SCR_020993
Other		
Human pancreatic cancer RNA and RPPA dataset	cBioportal	http://www.cbioportal.org/study/summary?id=paad_tcga_pan_can_atlas_2018